NE-CAT Communications

A Biannual Newsletter of the Northeastern Collaborative Access Team Summer 2012

Message from the Director

Steve Ealick

Year 2012 started with major events at NE-CAT. First, we installed the PILATUS 6MF detector on our 24-ID-C beamline. This brings the latest photon counting, noise-less, super fast detector technology to our user community. User feedback regarding the PILATUS 6MF has been very positive. I would like to thank the High-End Instrumentation grant 1S10RR029205 from NCRR for providing us funds to make this technology available to our users.

Second, after months of effort, intensive meetings and revisions, we have successfully submitted our "NE-CAT Center for Advanced Macromolecular Crystallography" P41 grant renewal application to NIGMS in May 2012. This renewal is expected to fund NE-CAT operations for the upcoming five years and also enable us to implement novel technologies in advanced micro-crystallography, computational tools and low-resolution crystallography. I am grateful to the NE-CAT Executive Committee and the Resource Advisory Committee for their valuable advice in preparing this grant application.

In addition, I am delighted at the enthusiastic letters of support we have received from all our current users and the PIs of our Driving Biomedical Projects, our collaborators, and our users. I firmly believe they will show reviewers the positive impact NE-CAT has made for our user community.

We have also made many improvements to our beamlines this year. You can read about these improvements later in this newsletter.

For further information on our beamline capabilities or to check out available beamtime, please visit our website at http://necat.chem.cornell.edu.

Beamline Developments

1. PILATUS 6MF installation on 24-ID-C

During early 2012, the PILATUS 6MF detector replaced the ADSC Q315 CCD detector on the 24-ID-C beamline. However, the CCD detector remains available to all groups. The detectors can be switched in a matter of hours.

A systematic comparison of data from the PILATUS 6MF and Q315 CCD detectors shows an improvement in data quality with the PILATUS 6MF detector. This is especially apparent at higher resolutions where Bragg peaks are weak and with crystals that inherently diffract weakly. We have also observed that the X-ray dose required to obtain a given diffraction resolution is smaller with the PILATUS 6MF detector compared to the Q315 CCD detector. This will help in prolonging the crystal life time on the beam. Similar anecdotal observations are also reported by many users who have used the PILATUS 6MF detector.

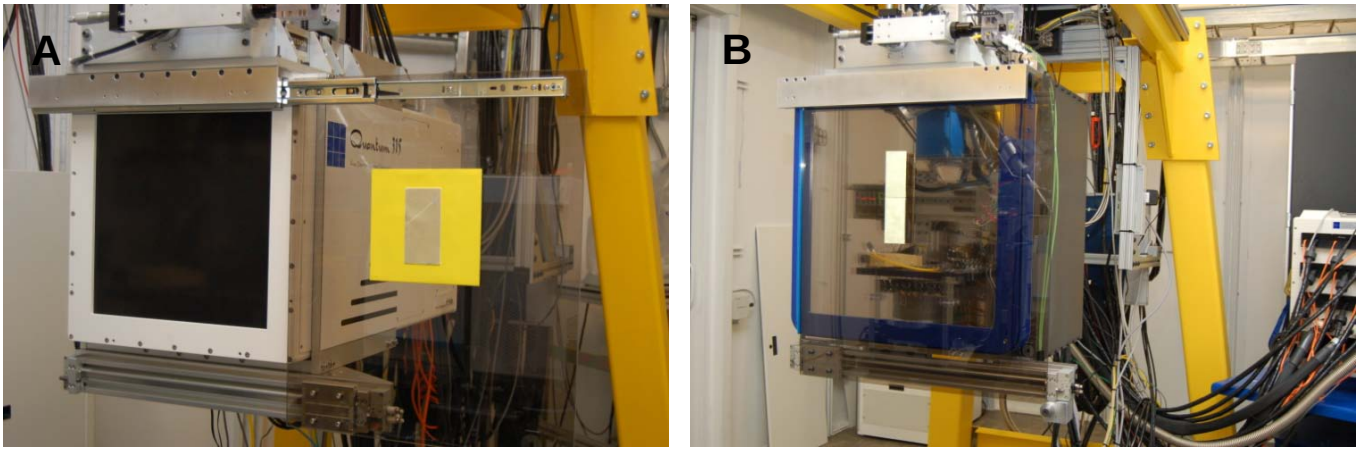

Fig. 1 A. New Guillotine installed on 24-ID-E and shown in the 'open' position. B. New Guillotine installed on 24-ID-C and shown in the 'closed' position.

The installation of the PILATUS-6MF on the 24-ID-C beamline required many hardware and software changes. First of all, it is important to protect the sensitive surface of the detector from accidental contacts. To protect our investment, a shield composed of Lexan was installed in front of the detector. Known colloquially as the "Guillotine", the curtain was manufactured on-site by Ed Lynch. The Guillotine automatically slides into place and covers the detector when the door to the hutch is opened or can be forced over the front of the detector using the "Guillotine" command on the auxiliary script.

After initial use, modifications were made to the Guillotine design and a similar curtain was installed on the ADSC Q315 detector in the 24-ID-E hutch during the May shutdown (Fig. 1A). The original Guillotine on the PILATUS 6MF was also replaced with the new version (Fig. 1B). Now the surfaces of both detectors are blocked from contact when users are inside the hutches. As a result of this new construction, the laser curtains have been removed.

The second hardware change to 24-ID-C may be easily missed by users. During the 2012-1 run, the PILATUS-6MF could not be moved any closer than 250 mm which equated to ~1.4 Å resolution at the Se edge. This limitation was a result of larger size of the PILATUS 6MF. At distances closer than 250 mm, the side of the detector would collide with the lid of the sample automounter storage dewar. Modifications were made to the sample automounter lid during the May shutdown. These modifications gained 100 mm in detector distance. The current closest detector distance is 150 mm. This improves maximum resolution at the Se edge by 0.4 Å.

The large size of the PILATUS still makes transverse motions of the detector hazardous. In order to prevent collisions or incidence of the direct beam on a module, the ability to move the detector up and down or side to side was, temporarily, de-activated on the 24-ID-C beamline control software. However, users requested the ability to lift the detector to accommodate large unit cells at close distances. The CONSOLE software was modified to allow movements of the PILATUS at one module intervals up and down. Users who need to translate the detector vertically can find this ability in the snapshot menu. The full range of motion (within safety limits) remains intact on the 24-ID-E beamline with its smaller ADSC Q315 detector.

The third hardware change should be invisible to users. At the beginning of March, it was noticed that at certain energies, the background was elevated in one module of the PILATUS 6MF. As a result, a site visit from Dectris was scheduled for module

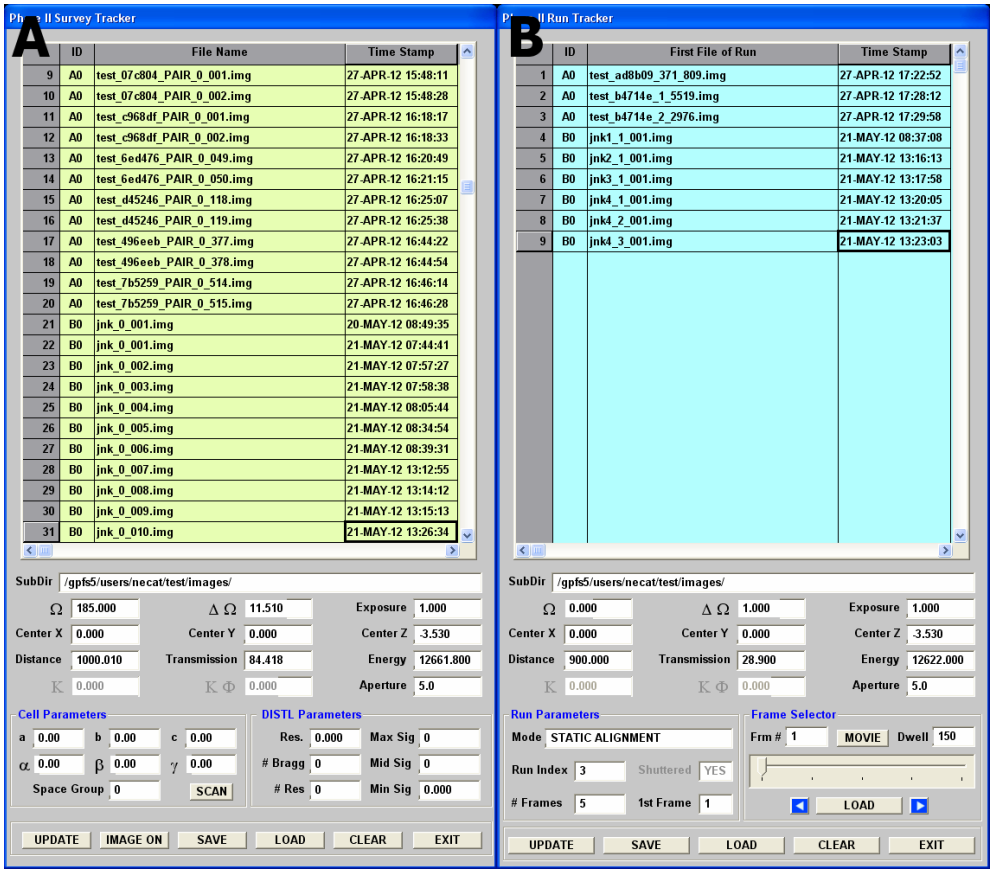

Fig. 2 A. Survey Tracker dialog filled with dummy samples. Clicking on a file name will select its diffraction image to be display on the ADSC viewer and the corresponding the bitmap of the crystal image to be displayed in a window next to the tracker dialog. B. Runs Tracker dialog filled with dummy samples.

replacement at the end of that month. During the visit, it was found that the module had a loose connection. The connector was replaced, solving the elevated background issue, but the module was not changed.

Overall, the installation and integration of PILATUS 6MF have been a great success and have been received very well by our user community. We will be implementing several novel data collection techniques with this detector during the upcoming months and years.

2. Fiber Optic Network Upgrade

The PILATUS detectors are known for rapidly generating copious amounts of data. The data must also be rapidly transported from the finite RAM disk to data storage disks. Fibre Channel (FC), using fiber optic cable, forms the communication backbone of our storage area network (SAN). Coincident with the installation of the PILATUS 6MF in January, a new 40-port 8 Gigabit FC switch was added to the SAN. With this addition, two old 12-port 2 Gigabit switches were taken out of service. This upgrade brings our FC fabric to a uniform 8 Gb/sec speed that is easily capable of handling all the data generated by the PILATUS 6MF.

3. Survey Tracker

Due to the speed at which images are collected by the PILATUS 6MF, it is no longer possible to see each image as it comes off the detector. To compensate, tracking has been implemented in the control software of both beamlines. There is a survey tracker for snapshots and a runs tracker for runs (Fig. 2).

The survey tracker takes a snapshot of every mounted crystal and stores a bitmap of the

Fig. 3 Drying Oven in the beamline work area.

image with the diffraction images. A table allows the user to select a filename and see both the crystal snapshot and the diffraction image on the screen. The table will also display RAPD-calculated statistics about chosen image. Finally, the entire table can be exported as an Excel spreadsheet and saved for future reference.

Similar to the survey tracker, the runs tracker will display a movie of all the images in a run as well as a bitmap of the crystal showing data collection locations. The table from the runs tracker can be exported as an Excel spreadsheet. Saved tables can also be reloaded into the tracker.

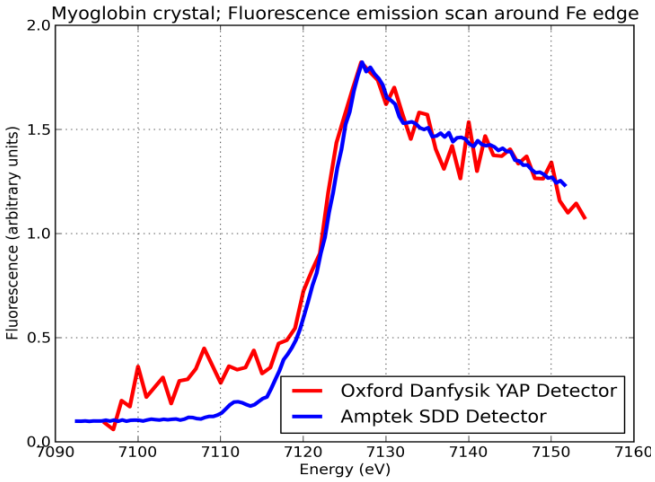

Fig. 4 Comparison of myoglobin EXAF scans taken at the Fe edge by the Oxford Danfysik (red line) and Amptek (blue line) Detectors. Clearly, the scan from the SDD Detector is much smoother than the scan from the YAP Detector.

4. Cluster Enhancement

To handle the high computional demands of data from the PILATUS detector, four additional compute nodes (64 cores) were added to our compute-cluster. Each new node has 64 GB of RAM while each old node only has 12 GB of RAM. The new nodes have more computational power than our existing nodes. These nodes were installed on the cluster during the May shutdown and initial tests show a 30% enhancement in processing speed.

5. Drying Oven

For those of you who came to NE-CAT in April, you may have noticed the new oven out on the beamline next to the C work area (Fig. 3). This oven can be used for efficiently drying cryopucks and any tools associated with using cryopucks. The oven temperature has been set to 110 ^{o}F. Cryopucks placed inside will be dry within 30 minutes.

6. Silicon Drift Detector Installed on 24-ID-C

During the 2011-3 run, an Amptek X-123SDD was installed on 24-ID-E (see the Winter 2011 newsletter). We are so impressed with its performance, that instead of moving that detector to 24-ID-C, as initially planned, a second X-123SDD has been purchased and installed on 24-ID-C. This silicon drift X-ray detector replaces the existing Cyberstar Scintillation Detectors fitted with Yttrium Aluminum Perovskit (YAP) crystals by Oxford Danfysik.. Compared to the YAP detector, SDD uses less X-ray dose to provide clean, fluorescence spectra (Fig. 4).

The Amptek X-123SDD is currently integrated into beamline only for EXAFS scans and users will be able to interact with it seamlessly using the auxiliary script. However, we plan to provide additional

controls for collecting Energy Dispersive X-ray emission spectrum in the future.

7. Remote Data Collection

As has been mentioned in previous newsletters, we have been working on adding remote data collection capability to our beamlines. We have made significant progress in this area to develop a novel and stable web-browser based remote data collection suite.

The web-based remote data collection interface interacts with the beamline controls and will work on any browser which supports HTML5. Users will be able to log in (Fig. 5A) and actively control a session (Fig. 5B) or watch data collection as an observer. More than one person in a group can be logged in during a session, but only a single user will have access to control the beamline. Users will be able to perform all tasks necessary to collect data just like on-site users, such as changing samples, aligning samples in real time using 3-click, vector scanning a crystal, auto-aligning the MD2, and changing aperture size.

Users will also be able to view diffraction images in both the data collection interface (Fig. 5C) or in a dedicated image viewer (Fig. 5D) which comes with the additional abilities such as determining the resolution of diffraction or zooming in on a particular area of the image, etc.

Users who need assistance will be able to talk to support staff via phone or video chat. Several users during the 2012-2 run aided in beta testing the system. It will be available to the entire user community in the 2012-3 run cycle.

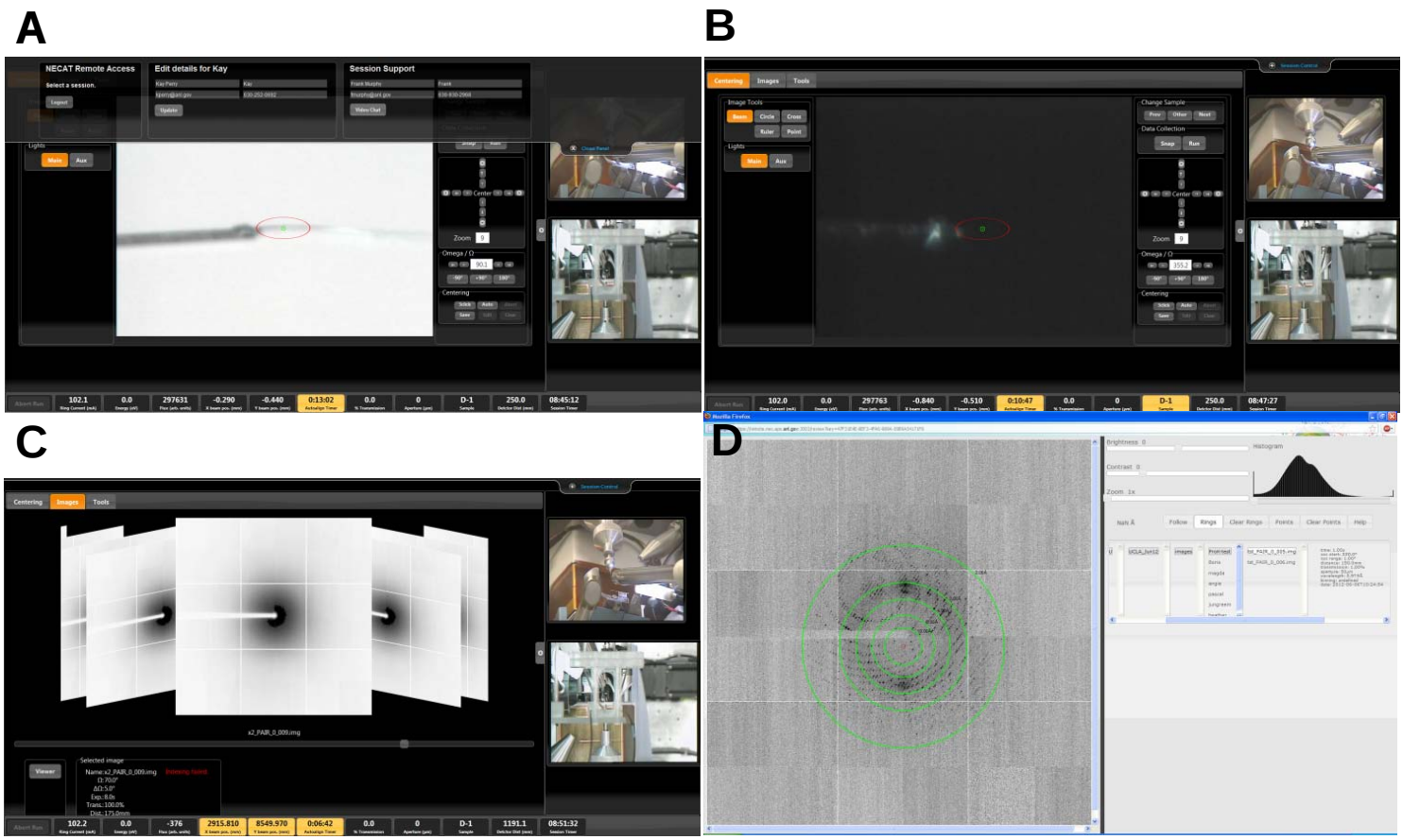

Fig. 5 Screenshots of the new Remote Data Collection Interface and Image Viewer. A. Log-in and Staff Support Dialog with a sample visible in the centering window. B. With the Log-in dialog closed, it is possible to see the controls for centering the sample and the live video feeds from the beamline. C. The Images tab of the data collection interface. D. The dedicated image viewer.

Research Highlights

Directing Carbon-Carbon Bond Forming Chemistry in Terpene Biosynthesis: Deciphering the Code

David W. Christianson, Roy and Diana Vagelos Laboratories, Department of Chemistry, University of Pennsylvania, Philadelphia, PA 19104-6323 USA

Terpenoid cyclases catalyze the most complex chemical reactions in biology, in that on average, two-thirds of the carbon atoms in a linear, achiral substrate undergo changes in chemical bonding and/or stereochemistry in a multi-step cyclization cascade leading to one or more products with multiple rings and stereocenters (1, 2). While the substrate pool for these enzymes is limited to only a handful of linear isoprenoids, the chemodiversity of terpenoid biosynthesis is extraordinary – more than 60,000 terpenoid natural products have been identified to date.

Terpenoid cyclases are unique among enzymes in that they are characterized not only by their reaction kinetics, but also by their product arrays. Some cyclases are high-fidelity enzymes that generate a single, exclusive product, whereas others are more promiscuous enzymes that generate multiple products. The evolution of terpenoid biosynthesis reflects nature's economical approach to synthetic diversity, in that facile evolution of a cyclase maximizes the potential product array, i.e., the chemodiversity, emanating from a limited substrate pool. Analysis of terpenoid cyclase crystal structures allows us to determine the structural features that guide the formation of one terpenoid product instead of another; in essence, the "code" that directs carbon-carbon bond formation in terpene biosynthesis.

We recently reported the first X-ray crystal structures of diterpene cyclases: taxadiene synthase (TXS) and *ent*-copalyl diphosphate synthase (CPS) (Fig. 6) (3, 4). TXS catalyzes the first committed step of Taxol biosynthesis in the Pacific yew (*Taxus brevifolia*). Taxol is a blockbuster cancer chemotherapy drug, and a complete understanding of its biosynthesis will enable its economical generation through synthetic biology approaches. The TXS structure is comprised of three α-helical domains, designated α, β, and γ. The C-terminal catalytic domain (the α domain) is a class I terpenoid cyclase, which binds and activates substrate geranylgeranyl diphosphate with a three-metal ion cluster. Surprisingly, the N-terminal domain (the β domain) and a third "insertion" domain (the γ domain) together adopt the fold of a vestigial class II terpenoid cyclase. A class II cyclase activates the isoprenoid substrate by protonation instead of ionization, but the general acid residue at the interface of the $\beta\gamma$ domains is mutated; hence, the class II domains of TXS are nonfunctional.

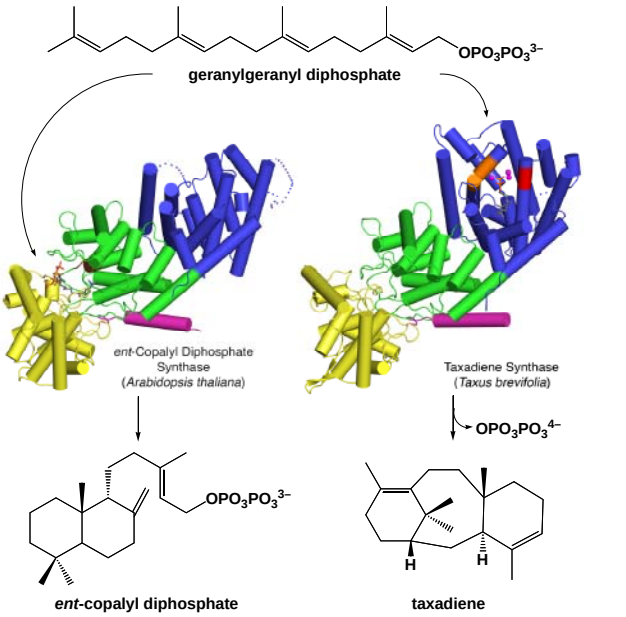

Fig. 6 Crystal structures of taxadiene synthase (TXS) and *ent*-copalyl diphosphate synthase (CPS) reveal identical protein folds. However, the active site of TXS is in the ☐ domain (blue), where it catalyzes the metal-dependent cyclization of geranylgeranyl diphosphate; the active site of CPS is at the interface of the ☐ and ☐domains (green and yellow, respectively), where it catalyzes the protonation-dependent cyclization of geranylgeranyl diphosphate.

The crystal structure of CPS, which generates a precursor to the labdane diterpene family of antibiotics, reveals an identical fold to that of TXS (Fig. 6) (4).

However, in this enzyme the α domain is catalytically inactive because it does not contain metal binding residues required for catalysis by a class I terpenoid cyclase. Instead, a general acid residue is present at the $\beta\gamma$ domain interface, so this diterpene cyclase is a functional class II cyclase. The modular domain architecture observed in TXS and CPS enables the facile evolution of alternative chemical strategies for catalyzing isoprenoid cyclization reactions, which maximizes chemodiversity in the evolution of terpenoid biosynthesis. These diterpene cyclase structures were determined by my accomplished postdoctoral fellow, Mustafa Köksal (Fig. 7).

In other work, we have recently determined the crystal structure of the bacterial sesquiterpene cyclase, epi-isozizaene synthase, and we have also determined the structures of several active site mutants (5). Mutant cyclases generate alternative cyclization products, and by correlating the three-dimensional structures of mutant active site contours with resultant product arrays, we are beginning to understand how a particular three-dimensional contour directs the cyclization cascade to form a particular product or array of products. This work was performed by my former graduate student Julie Aaron (Fig. 7).

In summary, the code for directing carbon-carbon bond forming chemistry in terpenoid cyclases is rooted in the particular cyclase domain that initiates the cyclization reaction. The multistep cyclization reaction sequence is encoded in the three-dimensional contour of the active site in the cyclase domain, which serves as a chaperone to ensure the correct sequence of carbon-carbon bond forming reactions. A full understanding of this biosynthetic code will ultimately enable protein engineering experiments in any cyclase scaffolding to generate desired terpenoids by design.

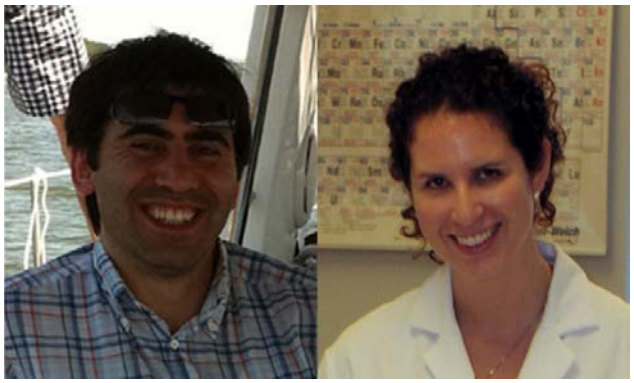

Fig. 7 Postdoctoral Fellow Mustafa Köksal (left) determined the first crystal structures of diterpene cyclases (3, 4). Former graduate student Julie Aaron (right) determined the crystal structure of epi-isozizaene synthase and its site-specific mutants (5). Julie is now Assistant Professor of Chemistry at DeSales University in Center Valley, Pennsylvania**.**

References

1. Christianson, D.W. (2006) Structural Biology and Chemistry of the Terpenoid Cyclases. **Chem. Rev.** *106*, 3412-3442.
2. Christianson, D.W. (2008) Unearthing the Roots of the Terpenome. **Curr. Op. Chem. Biol.** *12*, 141-150.
3. Köksal, M., Jin, Y., Coates, R.M., Croteau, R., Christianson, D.W. (2011) Taxadiene Synthase Structure and Evolution of Modular Architecture in Terpene Biosynthesis. **Nature** *469*, 116-120.
4. Köksal, M., Hu, H., Coates, R.M., Peters, R.J., Christianson, D.W. (2011) Structure and Mechanism of the Diterpene Cyclase *ent*-Copalyl Diphosphate Synthase. **Nature Chem. Biol.** *7*, 431-433.
5. Aaron, J.A., Lin, X., Cane, D.E., Christianson, D.W. (2010) Structure of Epi-Isozizaene Synthase from *Streptomyces coelicolor* A3(2), a Platform for New Terpenoid Cyclization Templates. **Biochemistry** *49*, 1787-1797.

Staff Activities

Our Computer Operations Manager, Amit Belani, completed his contract with NE-CAT in April 2012 and has moved on to a position at Fermi National Accelerator Laboratory. At NE-CAT, Amit contributed to cluster-computing and remote data collection interface development. We wish him the best in his new position.

Talks

Frank Murphy, “The future of automated data analysis at NE-CAT,” Life Science Council R&D Workshop. Argonne Guest House, Lemont, IL, May 2, 2012.

Kanagalaghatta Rajashankar, “Behind the beamstop crystallography,” Life Science Council R&D Workshop. Argonne Guest House, Lemont, IL, May 2, 2012.

Kanagalaghatta Rajashankar, “Comparison of diffraction data quality collected from a PAD and a CCD detector under identical conditions,” Life Science Council R&D Workshop. Argonne Guest House, Lemont, IL, May 2, 2012.

Surajit Banerjee, "Substrate-selective Inhibition of COX-2 by (R)-Profens," Aurigene Discovery Technologies Limited, Hyderabad, India, May 31, 2012.

Surajit Banerjee, "Dealing with Challenging Structural Biology Research at NE-CAT," Saha Institute of Nuclear Physics, Kolkata, India, June 6, 2012.

Jon Schuermann, “RAPD – Rapid Automated Processing of Data,” Partnering Data Collection and Reduction in the Beamline Environment, Tosteson Medical Education Center, Harvard Medical School, Boston, MA, July 27, 2012.

David Neau, “Automated Data Integration at NE-CAT,” Partnering Data Collection and Reduction in the Beamline Environment, Tosteson Medical Education Center, Harvard Medical School, Boston, MA, July 27, 2012.

Surajit Banerjee, Kanagalaghatta Rajashankar, “ When to do a MAD Experiment?” 2012 Annual Meeting of the American Crystallographic Association, Boston, Massachusetts, July 28 – August 1, 2012.

Malcolm Capel, Kanagalaghatta Rajashankar, Frank Murphy, Steven Ealick, “Integration of the Dectris PILATUS 6MF PAD detector at NE-CAT,” 2012 Annual Meeting of the American Crystallographic Association, Boston, Massachusetts, July 28 – August 1, 2012.

Kanagalaghatta Rajashankar, Igor Kourinov, Malcolm Capel, Steven Ealick, “Data Collection with 6 Million Detectors,” 2012 Annual Meeting of the American Crystallographic Association, Boston, Massachusetts, July 28 – August 1, 2012.

Frank Murphy, “Data Processing @ NE-CAT,” InterCAT Technical Workgroup Meeting, Advanced Photon Source, Lemont, IL, August 16, 2012.

Posters

Kanagalaghatta Rajashankar, Igor Kourinov, Malcolm Capel, and Steven Ealick, “Comparison of diffraction data quality collected from a PAD and a CCD detector under identical conditions,” Annual Meeting of the P41 Biomedical Technology Research Centers Principal Investigators, Rockville, MD, March 29 and 30, 2012.

Narayanasami Sukumar, “A Comprehensive Review on B12 Binding Proteins,” Gordon Research Conference on Diffraction Methods in Structural Biology, Lewiston, ME, July 15-20, 2012.

Surajit Banerjee, Amit Ketkar, MaroofZafar, Victor Marquez, Martin Egli, Robert Eoff, “Conformationally Restrained North-methanocarba-2’-deoxyadenosine Corrects the Error-Prone Nature of Human DNA Polymerase Iota,” 2012 Annual Meeting of the American Crystallographic Association, Boston, Massachusetts, July 28 – August 1, 2012.

Kay Perry, Tadhg Begley, Steven Ealick, “Structural Study of Isonitrile Synthase,” 2012 Annual Meeting of the American Crystallographic Association, Boston, Massachusetts, July 28 – August 1, 2012.

Igor Kourinov, Malcolm Capel, Surajit Banerjee, Frank Murphy, David Neau, Kay Perry, Kanagalaghatta Rajashankar, Jonathan Schuermann, Narayanasami Sukumar, Steven E. Ealick, "NE-CAT Crystallography Beamlines for Challenging Structural Biology Research," 2012 Annual Meeting of the American Crystallographic Association, Boston, Massachusetts, July 28 – August 1, 2012.

Publications

Banerjee, S., Christov, P. P., Kozekova, A., Rizzo, C. J., Egli, M., and Stone, M. P. (2012) Replication bypass of the trans-4-Hydroxynonenal-derived (6S,8R,11S)-1,N2-deoxyguanosine DNA adduct by the Sulfolobus solfataricus DNA polymerase IV, Chem. Res. Toxicol. 25, 422-435.

Ketkar, A., Zafar, M. K., **Banerjee, S.**, Marquez, V. E., Egli, M., and Eoff, R. L. (2012) A nucleotide analogue induced gain of function corrects the error-prone nature of human DNA polymerase iota, J. Am. Chem. Soc. 134(25):10698-705

Ren, A., **Rajashankar, K. R.**, and Patel, D. J. (2012) Fluoride ion encapsulation by Mg2+ ions and phosphates in a fluoride riboswitch, Nature 486, 85-89.

Gilbert, N. C., Rui, Z., **Neau, D. B.**, Waight, M. T., Bartlett, S. G., Boeglin, W. E., Brash, A. R., and Newcomer, M. E. (2012) Conversion of human 5-lipoxygenase to a 15-lipoxygenase by a point mutation to mimic phosphorylation at Serine-663, FASEB J. 26(8):3222-9

Lai, R. Y., Huang, S., Fenwick, M. K., Hazra, A. B., Zhang, Y., **Rajashankar, K. R.**, Philmus, B., Kinsland, C., Sanders, J. M., Ealick, S. E., and Begley, T. P. (2012) Thiamin pyrimidine biosynthesis in Candida albicans: a remarkable reaction between histidine and pyridoxal phosphate, J. Am. Chem. Soc. 134, 9157−9159.

Chan, R. T., Robart, A. R., **Rajashankar, K. R.**, Pyle, A. M., and Toor, N. (2012) Crystal structure of a group II intron in the pre-catalytic state, Nat. Struct. Mol. Biol. 19, 555-557.

Stokes-Rees, I., Levesque, I., **Murphy, F. V. t.**, Yang, W., Deacon, A., and Sliz, P. (2012) Adapting federated cyberinfrastructure for shared data collection facilities in structural biology, J. Synchrotron Radiat. 19, 462-467.

Zhao, B., Lei, L., Kagawa, N., Sundaramoorthy, M., **Banerjee, S.**, Nagy, L. D., Guengerich, F. P., and Waterman, M. R. (2012) A Three-dimensional Structure of Steroid 21-Hydroxylase (Cytochrome P450 21A2) with Two Substrates Reveals Locations of Disease-associated Variants. J. Biol. Chem. 287, 10613-10622.

Ekworomadu, M. T., Poor, C. B., Owens, C. P., Balderas, M. A., Fabian, M., Olson, J. S., **Murphy, F.**, Balkabasi, E., Honsa, E. S., He, C., Goulding, C. W., and Maresso, A. W. (2012) Differential Function of Lip Residues in the Mechanism and Biology of an Anthrax Hemophore. PLoS Pathog. 8, e1002559.

Cavalier, M. C., Kim, S. G., **Neau, D.**, and Lee, Y. H. (2012) Molecular basis of the fructose-2,6-bisphosphatase reaction of PFKFB3: Transition state and the C-terminal function, Proteins 80, 1143-1153.

Gu, S., Rumpel, S., Zhou, J., Strotmeier, J., Bigalke, H., **Perry, K.**, Shoemaker, C. B., Rummel, A., and Jin, R. (2012) Botulinum Neurotoxin Is Shielded by NTNHA in an Interlocked Complex, Science 335, 977-981.

Zong, Y., Zhang, B., Gu, S., Lee, K., Zhou, J., Yao, G., Figueiredo, D., **Perry, K.**, Mei, L., and Jin, R. (2012) Structural basis of agrin-LRP4-MuSK signaling, Genes Dev. 26, 247-258.

Vendeix, F. A., **Murphy, F. V. 4th.**, Cantara, W. A., Leszczynska, G., Gustilo, E. M., Sproat, B., Malkiewicz, A., and Agris, P. F. (2012) Human tRNA(Lys3)(UUU) Is Pre-Structured by Natural Modifications for Cognate and Wobble Codon Binding through Keto-Enol Tautomerism, J. Mol. Biol. 416, 467-485

Acknowledgements

NE-CAT is supported by grants from the former National Center for Research Resources (5P41RR015301-10), the National Institute of General Medical Sciences (8P41GM103403-10) and contributions from the following NE-CAT institutional members:

Columbia University
Cornell University
Harvard University
Massachusetts Institute of Technology
Memorial Sloan-Kettering Cancer Center
Rockefeller University
Yale University